Inclusion of a dithiadiazolyl radical in a seemingly non-porous solid

Varvara I. Nikolayenko, Leonard J. Barbour, Ana Arauzo, Javier Campo, Jeremy M. Rawson and Delia A. Haynes

Supplementary Information

All reagents employed in this study were purchased from commercial sources with no further purification. The L1 ligand was synthesized according to a previously reported method.[1]

Ligand Synthesis (L1)

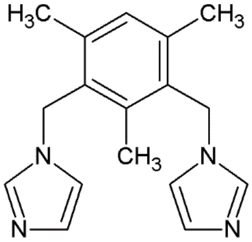

Solid 2,4-bis(chloromethyl)-1,3,5-trimethylbenzene (2.32 g, 10.7 mmol) was added to a solution of imidazole (6.71 g, 98.6 mmol) in 100 mL methanol. The mixture was heated under reflux at 70 °C. The reaction was followed by spotting of the product against the starting material on a TLC plate, and was found to be complete after 24 hrs. Excess solvent was removed under reduced pressure and gentle heating before precipitation of the product by adding an ample amount of a 10% K_2CO_3 solution. After washing with ethyl acetate, the pure white product was filtered and left to dry overnight. Yield: 1.532 g, 47%. H-NMR ($CDCl_3$, 300 MHz): δ 2.18 (3H, s, CH_3), 2.31 (6H, s, CH_3), 5.14 (4H, s, CH_2), 6.73 (2H, s, H_{im}), 7.01 (2H, s, H_{im}), 7.03 (1H, s, $H_{\mathbf{Bz}}$) 7.29 (2H, s, H_{im}) ppm.

Dithiadiazolyl radical synthesis

4-phenyl-1,2,3,5-dithiadiazolyl ($PhCNSSN^\bullet$) was prepared using the synthetic procedure previously reported by Robinson *et al*.[2]

Crystallisation

Crystals of **1** (the MeOH solvate of the metallocycle) were grown under solvothermal conditions in a programmable oven (Labotech, Ecotherm) (heated at 80 °C for 24 hrs before cooling to room temperature over a period of 36 hrs) by adding a solution 15.2 mg (0.089 mmol) of $CuCl_2 \cdot 2H_2O$ in 2 ml of methanol to a solution of 25 mg (0.089mmol) **L1** in 3 ml of methanol. Green block-shaped crystals suitable for single-crystal X-ray diffraction analysis (SCD) were obtained.

The solvent-free complex **1a** (apohost) was obtained by placing crystals of **1** at 100 °C under reduced pressure for 24 hrs. The apohost crystals were characterised by means of SCD, PXRD and thermal analysis.

Radical Loading

The loading of radical into **1a** was performed by sublimation under vacuum. A small sheared vial of **1a** (ca. 50 mg) was placed in a Schlenk tube containing ca. 50 mg of radical (**Figure S1**). The Schlenk was evacuated and heated at 80 °C to initiate sublimation of the radical. The guest-included crystals, **12**, were characterised by means of SCD, PXRD and thermal analysis, as well as EPR and SQUID.

Figure S1 Photographs of the experimental setup used to load the radical guest into **1a**.

Single-crystal X-ray diffraction

X-ray intensity data were recorded on a Bruker SMART APEX II[3] equipped with a Mo sealed tube source. The diffractometer employs an Oxford Cryosystems 700+ Plus cryostat to control the temperature of the sample. Data reduction was carried out by means of standard procedures using the Bruker software package SAINT[4]. Absorption corrections and correction of other systematic errors were carried out using SADABS[5]. All structures were solved by direct methods using SHELXS-16 and refined using SHELXL-16[6]. X-Seed[7] was used as the graphical interface for the SHELX program suite. Hydrogen atoms were placed in calculated positions using riding models.

Selected crystallographic data are given in **Table S1**.

Table S1 Crystallographic data for **1a** (apohost) and **12** (PhCNSSN$^\bullet$ inclusion) at two different temperatures.

	1a (apohost)		**12**	
Formula	$C_{34}H_{40}N_8Cl_4Cu_2$	$C_{34}H_{40}N_8Cl_4Cu_2$	$C_{19}H_{22}N_5Cl_2CuS_1$	$C_{34}H_{40}N_8Cl_4Cu_2$
Formula weight	829.64	829.65	939.38	821.59
Temperature/ K	100(2)	298(2)	100(2)	298(2)
Wavelength/ Å	0.71073	0.71073	0.71073	0.71073
Crystal system	Monoclinic	Monoclinic	Monoclinic	Monoclinic
Space group	$P2_1/c$	$P2_1/c$	$P2_1/c$	$P2_1/c$
a/ Å	8.327(2)	8.369(7)	8.360(5)	8.392(7)
b / Å	10.489(2)	10.600(9)	10.911(5)	10.831(8)
c / Å	22.224(5)	22.457(4)	22.138(2)	22.467(5)
β / °	98.546	98.774	99.147	99.10(3)
V/ Å^3	1919.6(1)	1969.2(5)	1993.89	2016.75
Z	2	2	2	2
SQUEEZE[8] Data are listed for all voids in the *P*1 unit cell	4	8	68 (34e per metallocycle)	84 (42e per metallocycle)

Powder X-ray diffraction

X-ray powder diffractograms were recorded on a Bruker D2 PHASER equipped with a Lynxeye 1D detector and Ni-filtered Cu Kα radiation (30 kV, 10 mA generator parameters; restricted by a 1.0 mm divergence slit and a 2.5° Soller collimator) with a 0.02° step width. All samples were first ground into a powder (using a mortar and pestle) and loaded onto zero background sample holders.

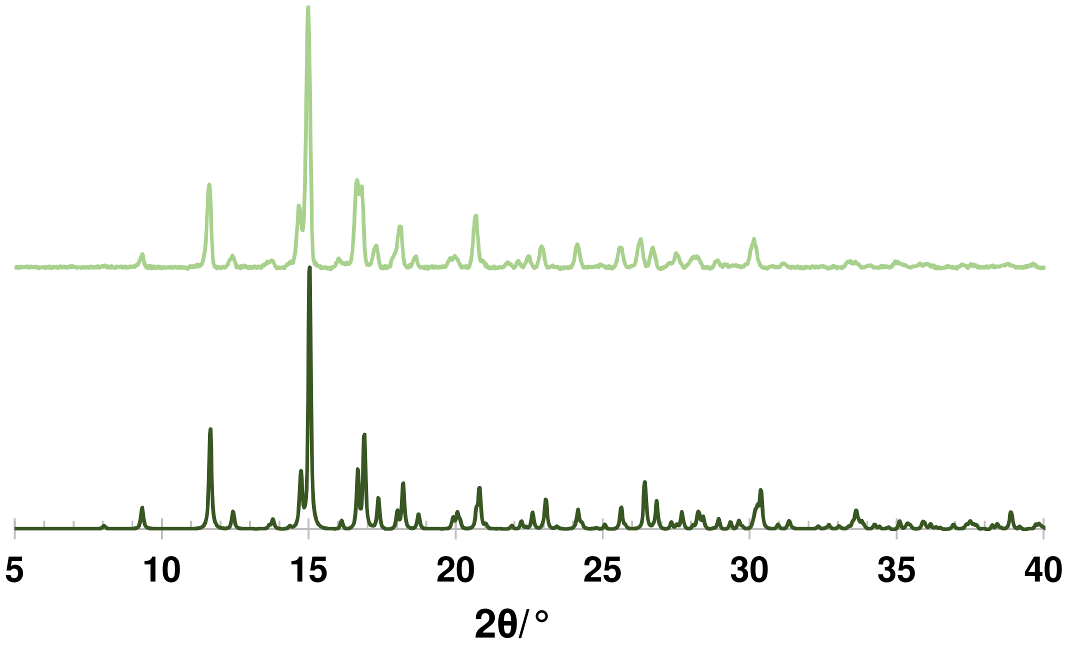

Figure S2 PXRD pattern of **1a** calculated from the SC structure (dark green), and the experimental pattern (light green), showing clearly that the SCD structure is representative of the bulk material.

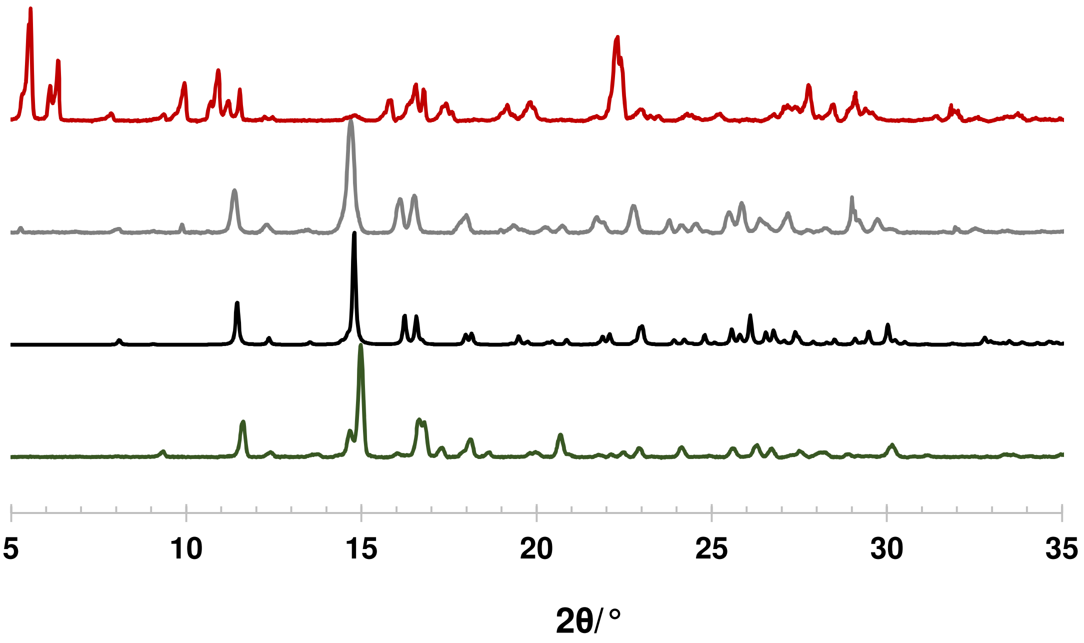

Figure S3 Experimental PXRD patterns of **1a** (green), **12** (black) and PhCNSSN• (red). The calculated PXRD pattern of **12** (grey) is included for comparison. It is clear that the structure of **1a** is maintained in **12**, and that no PhCNSSN• has sublimed on to the surface of the crystals of **1a**.

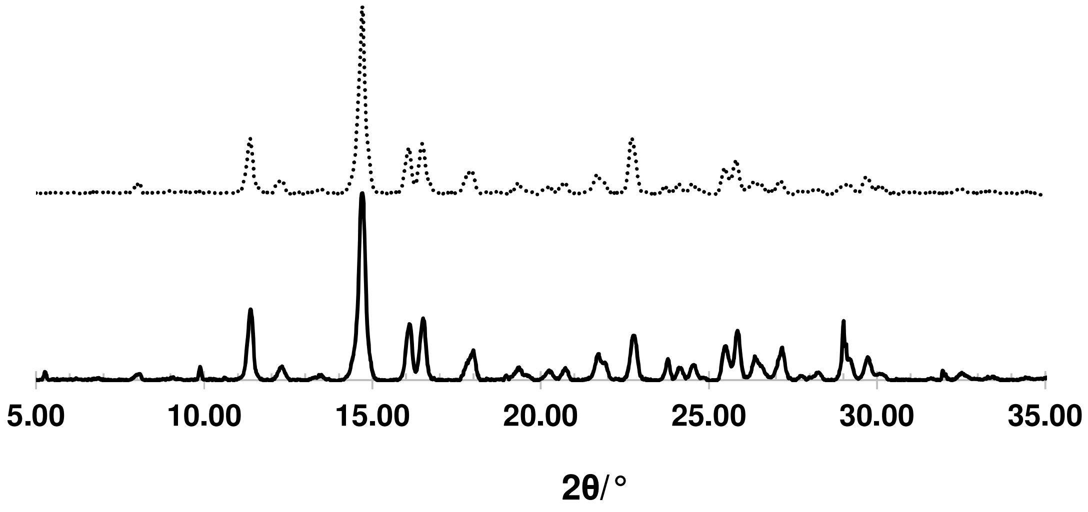

Figure S4 PXRD trace of **12** before (black) and after 1 month exposed to air in ambient conditions (dashed).

Thermogravimetric Analysis

Thermogravimetric analyses were carried out using a TA Instruments Q500 thermogravimetric analyser to record the weight loss of the sample as a function of temperature. The balance and sample were purged with dry N_2 gas flowing at rates of 50 and 70 cm^3 min^{-1}, respectively. Samples masses typically ranged from 2-7 mg and samples were heated at a constant rate of 10 °C min^{-1} from 25 °C to 600 °C. Thermograms were analysed using the TA Instruments Universal Analysis program.[9] **Figure S5** shows the overlaid TGA traces of **1** (green), **1a** (blue) and **12** (red). Desolvation of the methanol guest occurs before 100 °C while decomposition occurs after 250 °C.

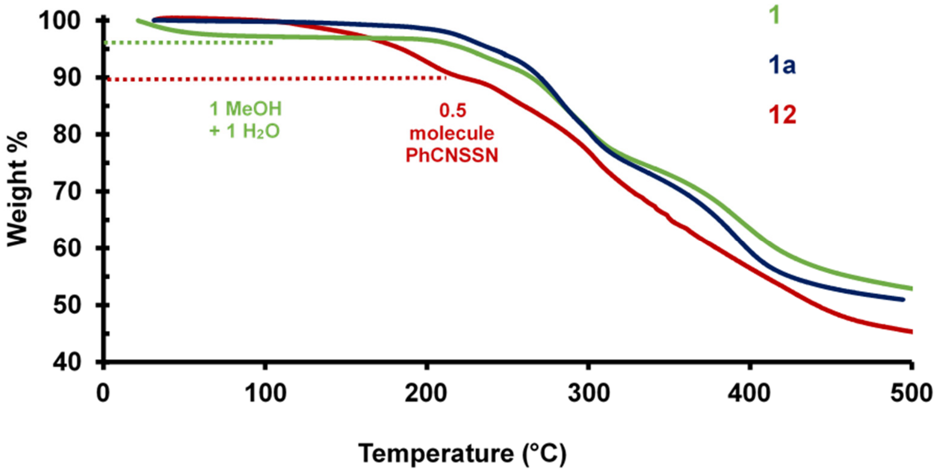

Figure S5 Overlaid TGA traces of the as-synthesised (**1**), activated (**1a**) and radical encapsulated (**12**) forms of the metallocycle.

1	mass loss 5.83 %	calculated mass loss for 1 MeOH + 1 H_2O	5.69 %
12	mass loss 9.23 %	calculated mass loss for ½ PhCNSSN	9.84 %

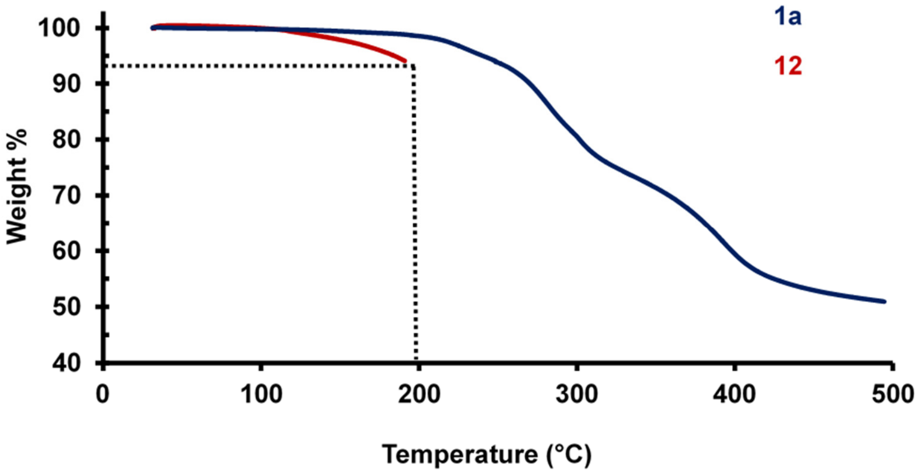

Figure S6 Overlaid TGA traces of **12** heated to 190 °C to expel the guest (green) and the same sample (red) after activation, heated to decomposition showing retention of metallocycle nature (compare to blue trace in **Fig. S5**).

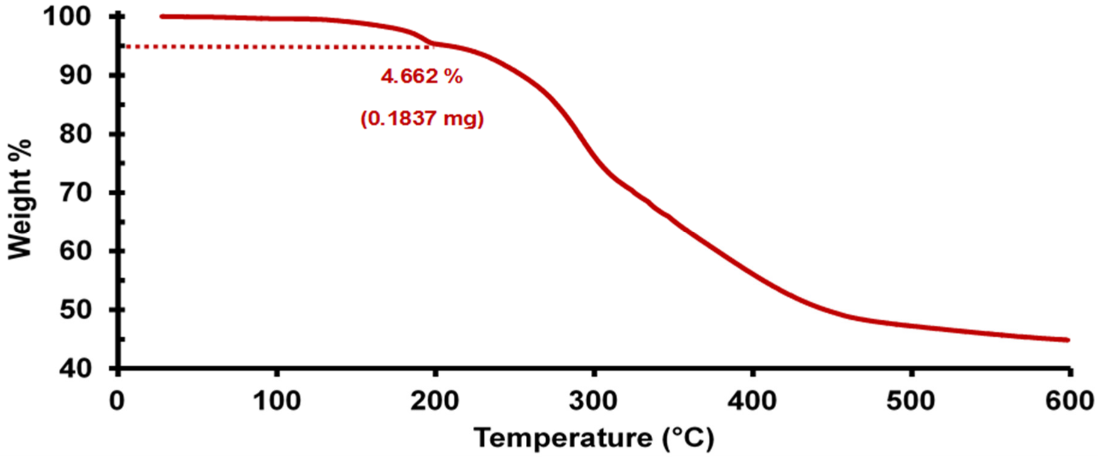

Figure S7 TGA of sample of **12** used for magnetic measurements. Expected mass loss for 24 % radical per metallocycle is 4.98 %.

Differential scanning calorimetry (DSC)

Differential scanning calorimetry was carried out using a TA Instruments Q100 differential scanning calorimeter. Samples were prepared by crimping the sample pan and lid (a pin hole was placed in the lid to prevent pressure build-up). A reference pan was prepared in the same manner for each analysis. Analyses were generally carried out in the temperature range -20-200 °C and a general experimental procedure consisted of three heating/cooling cycles while the heat flow into or out of the sample, relative to the reference, was measured as a function of time and temperature in a controlled atmosphere. N_2 gas, flowing at a rate of 50 ml min^{-1} was used to purge the furnace. The resulting thermograms were analysed using TA Instruments Universal Analysis program and figures were prepared with Microsoft Excel (**Figure S8**).

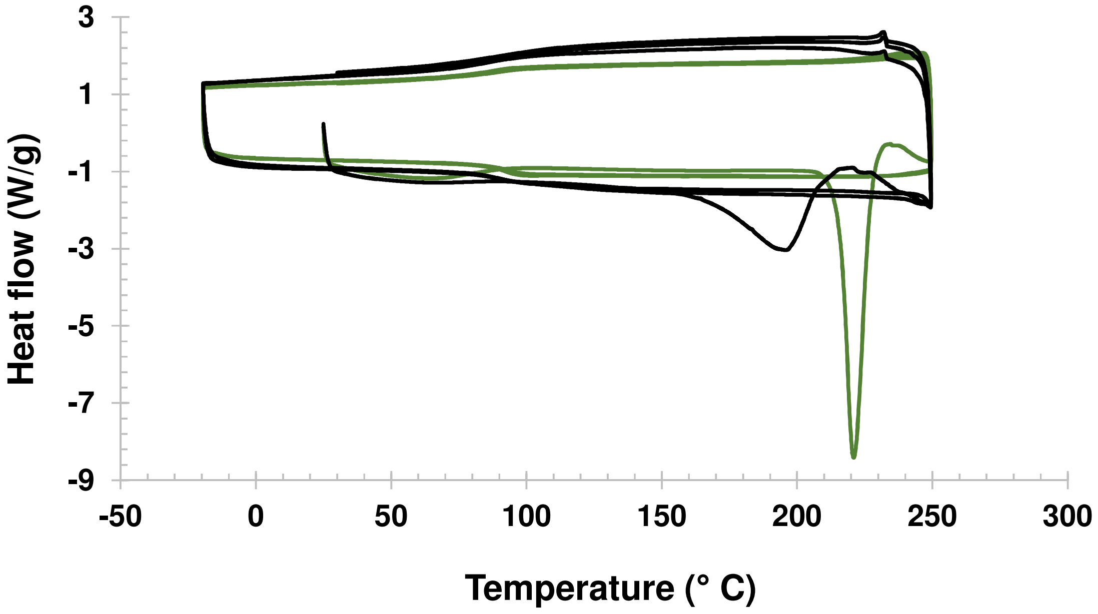

Figure S8 Overlaid DSC thermograms of **1a** (green) and **12** (black).

UV-visible Spectroscopy

Solid-state UV-visible absorption spectra were recorded for both **1a** and **12** using an Analytik Jena SPECORD 210 PLUS spectrophotometer. All measurements were performed at 25 °C to within ± 0.1 °C. Data were analyzed using the software package WinAspect PLUS 3.9.14 (**Figure S9**).[10]

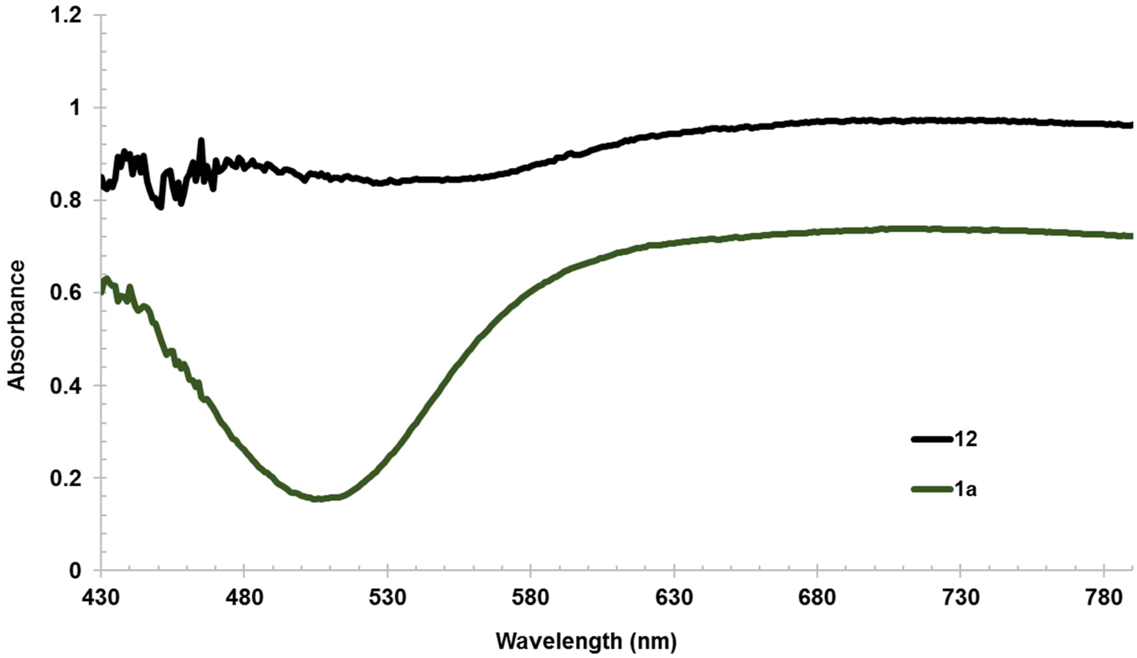

Figure S9 Overlaid UV-visible spectra of **1a** (green) and **12** (black).

IR Spectroscopy

IR spectra were measured on a Thermo Nicolet iS10 spectrometer with ATR attachment was used to measure IR spectra. A background scan was collected immediately before each sample scan.

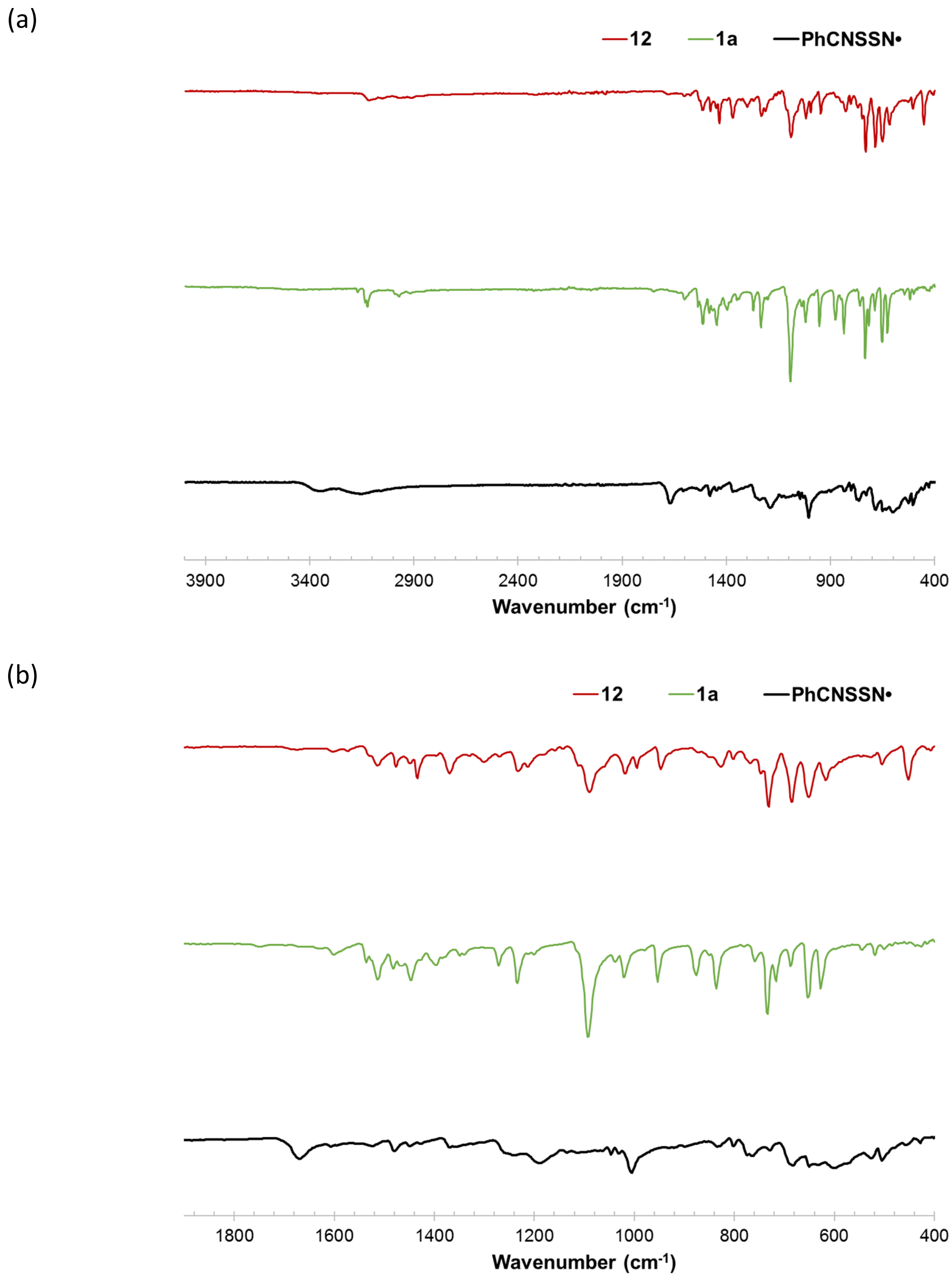

Figure S10 (a) IR spectra of **1a**, PhCNSSN$^{\bullet}$ and **12**. The broad peaks around 3400-3000 cm^{-1-} in PhCNSSN$^{\bullet}$ are possiblyNH-stretches due to small amounts of hydrolysis of the sample in air. Part (b) is an expanded view of the region between 1900 and 400 cm^{-1}, to allow better comparison.

EPR Spectroscopy

Solid-state EPR spectra were recorded on a Bruker EMXplus X-band EPR spectrometer (*ca*. 9.4 GHz) in the region 295 – 375 K. The temperature was maintained using a stream of dry nitrogen and a Eurotherm temperature controller. Anisotropic solid-state EPR spectra were simulated using PIP [M. Nilges, University of Ilinois] *via* the PIP4WIN GUI [J.M. Rawson, University of Windsor]. EPR spectral parameters for **1a** and **12** simulations are presented in Table S2 with EPR spectra simulations presented in **Figures S11** and **S12**.

Table S2 Spectral parameters used for EPR simulations.

1a	g_x	g_y	g_z	ΔH_{pp} (x)	ΔH_{pp} (y)	ΔH_{pp} (z)
295(1) K	2.042	2.085	2.240	25	33	55
315(1) K	2.042	2.090	2.248	22	35	59
335(1) K	2.042	2.078	2.245	27	28	50
355(1) K	2.043	2.087	2.245	22	36	55
375(1) K	2.043	2.083	2.248	22	36	55
12						
297(1) K	2.035	2.080	2.220	70	55	87
305(1) K	2.035	2.083	2.224	68	57	89
315(1) K	2.036	2.083	2.224	66	58	86
325(1) K	2.036	2.083	2.224	65	58	87
335(1) K	2.037	2.083	2.225	64	59	88
345(1) K	2.037	2.083	2.225	64	62	90
355(1) K	2.038	2.083	2.225	64	62	92
365(1) K	2.037	2.083	2.226	64	64	94
375(1) K	2.057	2.083	2.226	64	64	94

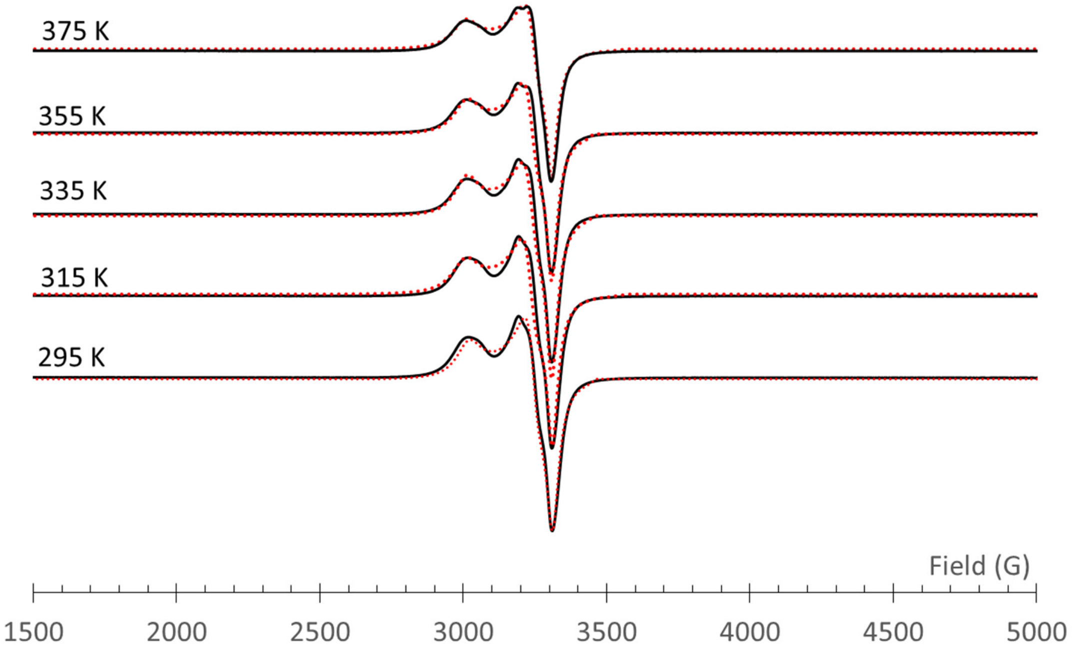

Figure S11 Variable temperature EPR spectra of **1a**; solid lines are spectra, dotted lines are simulations implementing the parameters given in **Table S2.**

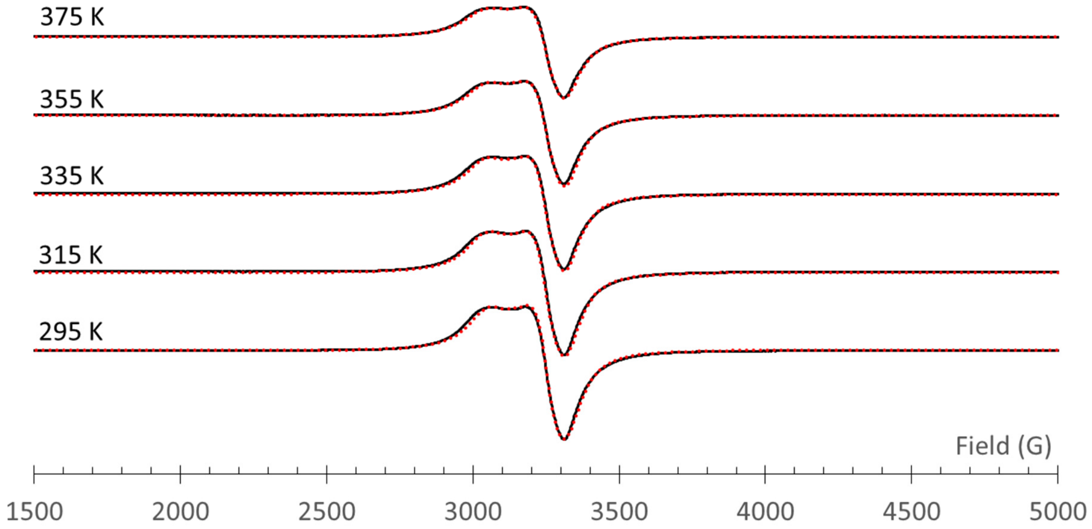

Figure S12 Variable temperature EPR spectra of **12**; solid lines are spectra, dotted lines are simulations implementing the parameters given in **Table S2**.

SQUID Magnetometry

Variable temperature and variable field dc susceptibility measurements were made on **1a** (31.27 mg) and **12** (18.50 mg). The data were corrected for the diamagnetism of the sample and sample holder.

Magnetization *vs* field plots for **1a** at 1.8 and 10 K (**Figure S13**) were replicated by the Brillouin function for two S = ½ radicals using g = 2.12 and a mean field correction term to take into account weak antiferromagnetic interactions (θ = -0.95 K, dotted line). A Curie-Weiss fit of the temperature dependence of χT for pristine **1a** exhibit similar parameters , C = 0.842 emu·K·mol^{-1} (corresponding to two S = ½ ions with g = 2.12) and θ = -2.0 K, to those determined from the M *vs* H data in the 1.8 – 10 K range.

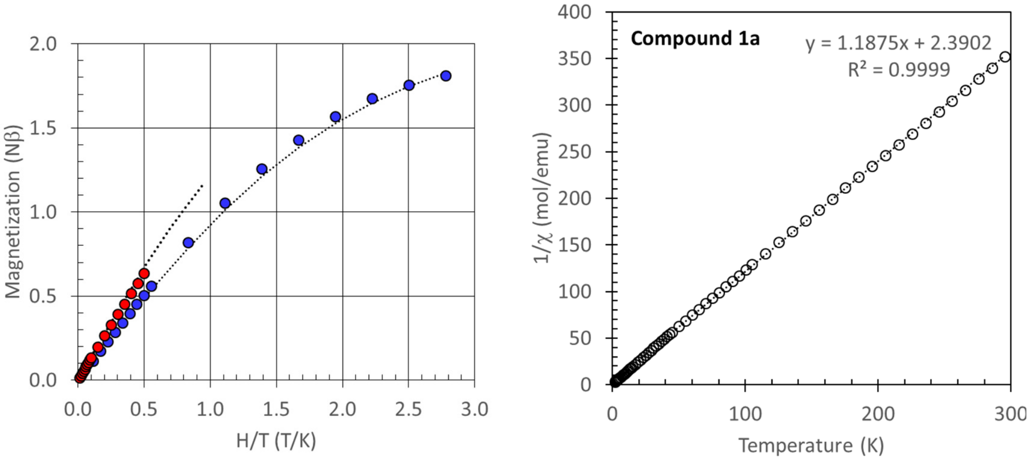

Figure S13 (left) M *vs* H/T for **1a** at 10 K (red data) and 1.8 K (blue data) with fits to the Brillouin function for both measurements (two S = ½ with g = 2.12 and θ = -0.95 K) represented as dotted lines; (right) Temperature dependence of 1/χ for **1a** (1.8 – 300 K) (C = 0.842 emu.K.mol^{-1}), θ = -2.0 K).

For **12** TGA measurements on the sample studied by SQUID magnetometry revealed a loading of ca. 24 % radical (see **Figure S7**). On analysis of the data, two distinct regions were observed (**Figure S14**). In the high temperature region (T > 50 K) the sample follows Curie-Weiss behaviour with C = 0.945 emu K mol^{-1} [2 × S = ½ with g = 2.15 (0.864 emu K mol^{-1}) and 24% S = ½ with g = 2.01 (0.09 emu K mol^{-1})] and θ = -5.5 K. In the low temperature region (T < 20 K) the sample follows Curie-Weiss behaviour with C = 0.772 emu K mol^{-1} and θ = -0.63 K. The decrease in C upon cooling is consistent with antiferromagnetic coupling between **1a** and PhCNSSN$^{\bullet}$ radicals and/or radical-radical coupling between guest molecules. Given the incomplete loading of radicals into the channels, host-guest interactions are more likely and supported by DFT calculations of exchange interactions.

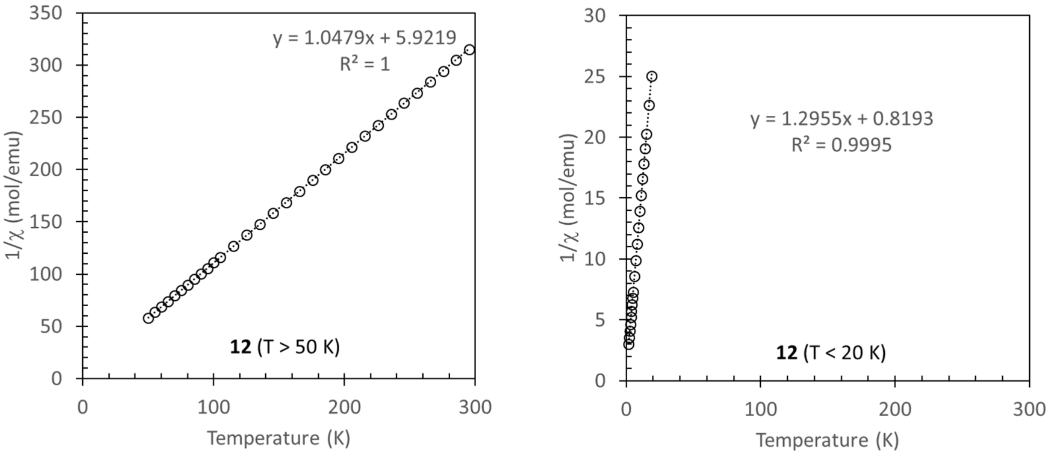

Figure S14 1/χ *vs* T for **12**: left T > 50 K; right T < 20 K.

DFT Calculations

Single point calculations were undertaken on PhCNSSN included in the **1a** framework based on the crystallographically determined structure. The position of the PhCNSSN radical was selected to be one of the two possible sites arising from crystallographic disorder. The lack of crystallographic symmetry afforded two sets of radical…Cu contacts which were expected to lead to different magnetic exchange couplings and the strength of the exchange coupling was determined by computing the energy of the triplet (T) and broken symmetry singlet (BSS) configurations using the method of Yamaguchi[11] in which the exchange coupling is given by:

$$J = -\frac{E_T - E_{BSS}}{<S^2>_T - <S^2>_{BSS}}$$

Where E_T and E_{BSS} correspond to the energies of the triplet and broken symmetry singlet configurations respectively whereas $<S^2>_T$ and $<S^2>_{BSS}$ refer to the expectation values of the triplet and broken symmetry singlet states. With three spin active centers (radical plus two Cu^{2+} ions) two sets of calculations were undertaken in order to compute the two independent exchange couplings. In each set of calculations one of the two Cu^{2+} ions was replaced by a diamagnetic Zn^{2+} ion. Previous work[12] by Novoa and Turnbull have provided good estimates of exchange couplings in copper-based coordination complexes using the B3LYP functional and a mixed basis set in which 6-31G(p) was used for all atoms except the metal centers which implemented Ahlrichs' double-zeta valence polarized (DZVP) basis set. In the current studies we employed the 6-31G*+ basis set for all non-metals and a triple zeta valence polarized basis set for Cu(Zn) atoms. The close S…Cu contact distances for each interaction and computed exchange couplings are presented in **Table S3** with a summary schematic of the Cu…S distances of the PhCNSSN radical within the **1a** framework shown in **Figure S15**. All computations were carried out using Jaguar 9.0 (release 18)[13], stipulating the ioss = 1 command for the broken symmetry singlet and with an initial guess based on setting the metal ions with a +2 charge and Cl^- anions with a 1- charge. The ligand **L1** in the host shows some structural disorder which was modelled over two sites. Both possible host conformations (major and minor) were examined.

Table S3 S…Cu contact distances and calculated exchange couplings (*J*), where *J*(major) is calculated using the geometry of the major component of the disorder in the structure, and *J*(minor) using the minor component.

Exchange interaction	Cu….S /Å	J/cm^{-1} (major)	J/cm^{-1} (minor)
J_1	3.74, 3.75	-10.3	-1.1
J_2	3.82, 4.87	-10.5	-12.3

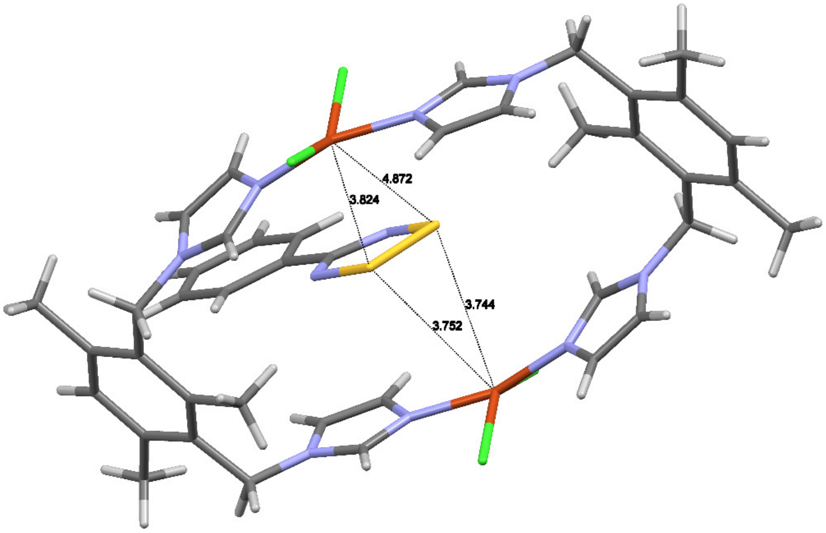

Figure S15 Diagram indicating the Cu…S distances used in the calculations on **12**.

References

1. L. Dobrzańska, G. O. Lloyd, H. G. Raubenheimer, L. J. Barbour, *J. Am. Chem. Soc.*, 2006, **128**, 698-699.
2. S. W. Robinson, D. A. Haynes and J. M. Rawson, *CrystEngComm.*, 2013, **15**, 10205.
3. SMART Data Collection Software, Version 5.629, Bruker AXS Inc., Madison, WI, 2003.
4. SAINT Data Reduction Software, Version 6.45, Bruker AXS Inc., Madison, WI, 2003.
5. SADABS, Bruker AXS Inc., Madison, WI, 2014.
6. G. M. Sheldrick, *Acta Crystallogr., Sect. C*, 2015, **71**, 3.
7. G. M. Sheldrick, *Acta Crystallogr., Sect. A*, 2008, **64**, 112.
8. A. L. Spek, A. L. *J. Appl. Crystallogr.* **2003**, *36*, 7.
9. Universal Analysis 2000, Version 4.5A, TA instruments , Waters-LLC, 2007.
10. WinASPECT PLUS, Version 3.9.32.0, analytic Jena AG, 2002.
11. K. Yamaguchi, H. Fukui and T. Fueno, *Chem. Lett.*, 1986, **625**, 21; K. Yamaguchi, Y. Takahara, T. Fueno and and K.N. Houk. *Theo. Chim. Acta*. 1988 **73**, 337; S. Yamanaka, M. Okumura, M. Nakano and K. Yamaguchi, *J. Mol. Struct.* 1994, **310**, 205.
12. A. Shapiro, C.P. Landee, M.M. Turnbull, J. Jornet, M. Deumal, J.J. Novoa, M.A. Robb and W. Lewis, *J. Am. Chem. Soc.*, 2007, **129**, 952; F.F. Awwadi, S.F. Haddad, M.M. Turnbull, C.P. Landee and R.D. Willett, *Cryst.Eng.Comm.*, 2013, **15**, 3111; L. Li, M.M. Turnbull, C.P. Landee, J. Jornet, M. Deumal and J.J. Novoa, *Inorg. Chem.* 2007, **46**, 11254.
13. Jaguar 9.0, Schrödinger LLC: A.D. Bochevarov, E. Harder, T.F. Hughes, J.R. Greenwood, D.A. Braden, D.M. Philipp, D. Rinaldo, M.D. Halls, J. Zhang and R.A. Friesner, *Int. J. Quantum Chem*., 2013, **113**, 2110.